Brm *hnRNA is undetectable in the Brm-deficient cell lines*

To elucidate molecular mechanisms of post-transcriptional suppression of the *Brm* gene in Brm-deficient cell lines, we performed RT–PCR analysis to detect parts of *Brm* hnRNA using two primer pairs covering 5′-region (third intron and fourth exon) and 3′-region (32nd intron and 33rd exon) of the primary transcript. Both regions were clearly detectable in MDA-MB435 and HeLa-S3 cells (Figure 2). However, in most of the Brm-deficient cell lines neither regions were detected, and only in NCC-IT, the trace of RT–PCR product was detectable. These results indicate that there is only marginal amounts of *Brm* primary transcripts in Brm-deficient cell lines immediately after the transcription, suggesting that post-transcriptional suppression of the *Brm* gene starts at very early stages. The presence of a small amount of hnRNA in NCC-IT cells would be reflecting a rather high level of *Brm* transcription as judged by the nuclear run-on assay (Figure 1c), and further suggests that post-transcriptional suppression of *Brm* may be operating also in later stages, such as nuclear export or mRNA instability.

Transient treatment with HDAC inhibitors induces prolonged expression of Brm protein in Brm-deficient cell lines

In all the Brm-deficient cell lines tested here, the *Brm* gene locus seemed to be at least not largely arranged, as the fourth and 34th exons of *Brm* gene were detectable by genomic PCR, and also because nuclear run-on transcription assays showed both initiation and elongation of the *Brm* transcript proceed efficiently (Figure 1b and c). Considering that the *Brm* gene expression is epigenetically regulated in these cell lines, several reagents were screened for their ability to induce Brm protein expression, and we found that HDAC inhibitor such as FK228 (Nakajima *et al.*, 1998; Furumai *et al.*, 2002) or CHAP31 (Komatsu *et al.*, 2001) can efficiently induce Brm protein production in all seven Brm-deficient tumor cell lines (Figrue 3, Table 2). Both FK228 and CHAP31 target class I HDACs including HDAC1 and HDAC2. Induction of Brm protein production was always accompanied by increased expression of *Brm* mRNA, as monitored by RT–PCR

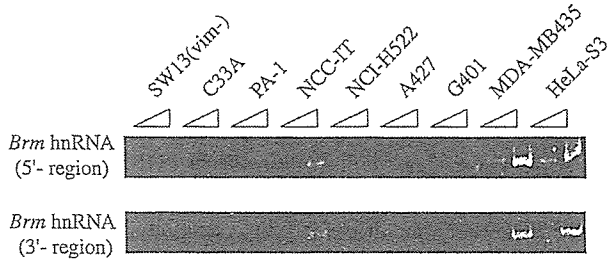

Figure 2 RT–PCR analyses to detect 5′- and 3′-region of *Brm* hnRNA in the seven Brm-deficient cells and two Brm-expressing cells. For each cell line, the products generated from 35 and 40 PCR amplification cycles were shown

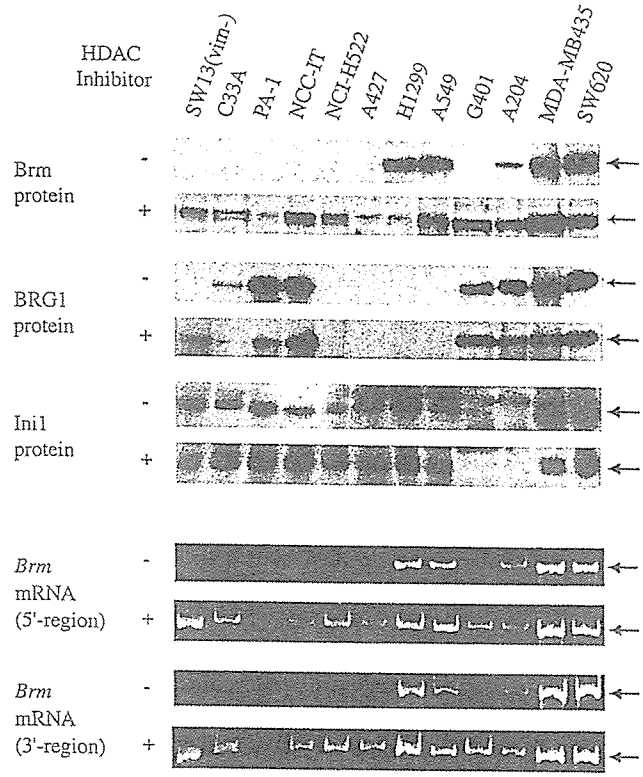

Figure 3 Gene expression patterns in several human tumor cell lines before and after the treatment of HDAC inhibitors. Cells were grown in DMEM in the absence(−) or the presence(+) of HDAC inhibitors at the concentrations listed on Table 2 for 3 days. Under these conditions, no growth inhibition or cytotoxic effects were observed. All the cultures were grown in the absence of the inhibitor for additional 24 h, and were disrupted for preparing total cell protein under denaturing conditions or total RNA. Brm, BRG1, and Ini1 protein expression was analysed by Western blotting (upper panel), and *Brm* mRNA was detected by semiquantitative RT–PCR using two independent pairs of primers (lower panel). Protein bands (arrows) of Brm (190 kDa), BRG1 (190 kDa), and Ini1 (47 kDa) were detected by immunostaining with the corresponding specific antisera

(Figure 3). In contrast, Brm protein levels in Brm-expressing cell lines were not affected significantly by the HDAC inhibitor treatment (Figure 3). As the initiation and elongation of the *Brm* transcript proceeds efficiently in all the Brm-deficient cell lines, this induction cannot be explained by the direct effect on the transcription of the *Brm* gene. Therefore, these results suggest that HDAC inhibitors indirectly attenuate post-transcriptional suppression of *Brm* through induction of other genes.

When BRG1 and Ini1 were analyzed by Western blotting of the same cell lysates, production of BRG1 in BRG1-deficient cell lines was not induced after the treatment of HDAC inhibitors, and similar results were obtained with respect to Ini1 (Figure 3, Table 2). The only one exception was SW13(vim-) cells, in which production of BRG1 protein was induced by the HDAC inhibitors. Post-transcriptional suppression of *BRG1* observed specifically in SW13(vim-) (Yamamichi-Nishina *et al.*, 2003) is also shown to be released by this

Table 2 Expression of Brm, BRG1, In:1 proteins, and mosaic colony ratio of several human tumor cell lines, before and after HDAC inhibitor treatment

Cell line	*FK228 (ng/ml)*	*Detection of Brm mRNA*		*Protein expression*						*Mosaic colony ratio (%)*	
		Un	*T*	*Brm*		*BRG1*		*Inil*		*Un*	*T*
				Un	*T*	*Un*	*T*	*Un*	*T*		
SW13(vim−)	0.7	−	+	−	+	−	+	+	+	**82**	**15**
C33A	[a]	−	+	−	+	+	+	+	+	**73**	**58**
PA-1	0.5	−	+	−	+	+	+	+	+	**79**	**45**
NCC-IT	1.6	−	+	−	+	+	+	+	+	**83**	**24**
NCI-H522	1.0	−	+	−	+	−	−	+	+	**91**	**23**
A427	1.0	−	+	−	+	−	−	+	+	**78**	**18**
H1299	1.5	+	+	+	+	+	+	+	+	15	NT
A549	1.3	+	+	+	+	+	+	+	+	30	NT
G401	1.0	−	+	−	+	+	+	−	−	*66*	*73*
A204	1.3	+	+	+	+	+	+	−	−	*75*	*79*
MDA-MB435	1.0	+	+	+	+	+	+	+	+	19	17
SW620	1.3	+	+	+	+	+	+	+	+	12	NT
HeLa-S3	1.0	+	+	+	+	+	+	+	+	29	28

NT = not tested; Un = untreated cells; T = cells after the treatment with HDAC inhibitor for 3 days. Cells were grown for 24 h in the absence of the inhibitor prior to Western blotting analysis or the mosaic colony assay. [a]Owing to cytotoxic effects of FK228, 5.5 nM of CHAP31 was used instead

reagent. These results suggest that deficiency in BRG1 expression can be caused by the several different mechanisms, in contrast to a rather common mechanism of post-transcriptional suppression observed in Brm-deficient cell lines. Therefore, it is difficult at present to propose a simple model, which explain why there are so frequent cases of concomitant loss of Brm and BRG1 protein in human tumor cell lines and original tumors (Table 1; Wong *et al*., 2000; DeCristofaro *et al*., 2001; Reisman *et al*., 2002).

Next, to examine how HDAC inhibitors influence expression of Brm, we monitored the kinetics of Brm protein expression in SW13(vim-) and A427 cells after HDAC inhibitor treatment (Figure 4). In both cell types, Brm levels were unchanged for 1–3 days after removal of the inhibitor, and significant expression was detected until day 7, whereas Brm levels decreased considerably on day 10, and became marginal on day 14. RT–PCR analysis of SW13(vim-) cells revealed that kinetics of *Brm* mRNA was similar to that of Brm protein level: *Brm* mRNA was strongly induced by the HDAC inhibitor treatment (Figure 4). Since production of primary *Brm* transcript in untreated SW13(vim-) was efficient (Figure 1b), it is indicated that transient treatment with HDAC inhibitors would repair attenuated processing of the *Brm* primary transcript into mRNA.

The major targets of HDACs are acetylated histones in the chromatin. Therefore, addition of HDAC inhibitors should rapidly increase acetylation of histones, and removal of HDAC inhibitors would be expected to reduce amounts of acetylated histones rapidly to levels similar to those of untreated cells. To monitor this process, we analyzed acetylated histone H3 in SW13(vim-) cells by Western blot analysis, because untreated SW13(vim-) contain only a low level of this modified form of histone H3 (Figure 4). When SW13(vim-) cells were treated with FK228, levels of acetylated H3 were elevated dramatically as expected,

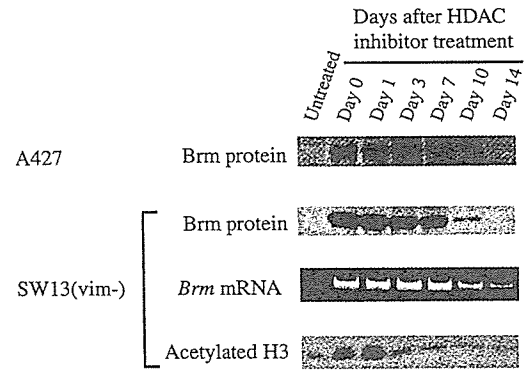

Figure 4 Time course of Brm protein expression in A427 and SW13(vim-) cells after HDAC inhibitor treatment. These Brm-deficient cell lines were grown for 3 days in the presence of FK228 (1.0 ng/ml for A427 and 0.7 ng/ml for SW13(vim-)). After removing FK228 (day 0), each cell line was grown for additional 1 to 14 days (days 1–14), and whole-cell extracts or total RNA were prepared on the indicated day. For SW13(vim-) cells, acetylated histone H3 and *Brm* mRNA levels were also quantified. Total cellular extracts (20 μg each) were immunoblotted with anti-Brm or antiacetylated histone H3 antibody. Total RNA (300 ng) was used for RT–PCR of *Brm* mRNA

and this increase was sustained for 1 day after removal of FK228, possibly due to residual HDAC inhibitor in the treated cells. However, levels of acetylated H3 soon dropped to the original level: this decrease was much more rapid than that of Brm protein.

It was recently reported that Brm protein is a target of histone acetyl transferases, and that treatment with HDAC inhibitors such as trichostatin A causes efficient acetylation of exogenously introduced Brm protein, with a concomitant increase in the exogenous Brm level (Bourachot *et al*., 2003). We believe that the prolonged expression of Brm protein after HDAC inhibitor treatment is not explained by induced acetylation of endogenous Brm protein. It is because

SW13(vim-) cells on days 3–14, where HDAC inhibitor retains no activity judged by the level of acetylated histone H3, still synthesize a large amount of Brm protein.

Brm protein expressed in response to HDAC inhibitors is functional and supports retroviral gene expression

Transgene expression by an MuLV-based retrovirus vector is rapidly silenced in human tumor cell lines deficient in Brm, and this rapid silencing can be attenuated by exogenous transduction of Brm (Mizutani *et al*., 2002). In our previous study, we developed an assay to allow sensitive quantification of retroviral gene silencing that occurs within 4 days after the infection of LacZ virus, where the degree of retroviral gene silencing is defined as the 'mosaic colony ratio'. To examine whether Brm protein induced by HDAC inhibitor is biologically functional, we performed this assay to check the retroviral gene silencing, with the cell lines before and after HDAC inhibitor treatment.

Without the HDAC inhibitor treatment, the mosaic colony ratios of Brm-deficient cell lines were high (66-91%) and those of Brm-expressing cell lines were low, confirming our previous finding that functional Brm, but not BRG1, is essential for maintenance of gene expression by MuLV-based retrovirus (Table 2). We observed one clear exception: A204 cells, which do not produce functional Ini1 protein but do express Brm protein, have the very high mosaic colony ratio of 75%. We would like to expand our previous model and conclude that the functional Brm-type SWI/SNF complex containing the Ini1 subunit is essential for stable expression of retrovirus.

When the seven Brm-deficient cell lines were treated with HDAC inhibitors for 3 days and cultured 1 day in the absence of the reagent, all expressed Brm protein, as shown in Figure 3. We performed the mosaic colony assays with these Brm-induced cells, and six cell lines showed significant reduction of mosaic colony ratio, indicating that they acquired the ability to maintain MuLV-based retrovirus expression (Table 2). These results indicate that Brm protein produced in response to HDAC inhibitors is biologically functional. The one exception was G401 cells, whose mosaic colony ratio after the treatment was similar to that of untreated cells. This observation can be explained by the fact that functional Brm-type SWI/SNF complex would not be formed in Ini1-deficient G401 cells, even if Brm protein is induced. Together with the finding of the high mosaic colony ratio of A204 cells described above, the idea that the Ini1 subunit is essential for stable retroviral gene expression is further reinforced.

The kinetics of induced Brm protein expression revealed that SW13(vim-) and A427 cells retain very low expression of Brm, even 2 weeks after the removal of FK228 (Figure 4). When these cells were transduced with a LacZ virus for the mosaic colony assay, SW13(vim-) and A427 cells still showed significant suppression of retroviral gene silencing with mosaic colony ratios of 48 and 41%, respectively.

Transient treatment with HDAC inhibitors suppresses oncogenic potential of Brm-deficient cell lines

From the viewpoint of oncogenic potential, we next investigated the effect of prolonged epigenetic induction of Brm protein. To evaluate invasive potential, we first performed a tumor invasion assay. Of the seven Brm-deficient cell lines examined, only PA-1 exhibited clear invasion in collagen gel. PA-1 cells were treated with FK228 for 3 days, grown for an additional 24 h in the absence of FK228, and injected into collagen gel. In the embedded culture, untreated PA-1 cells showed clear invasion on days 7–10, whereas FK228-treated PA-1 cells showed drastically reduced invasive activity (Figure 5a). When FK228-treated PA-1 cells were grown as monolayer cultures for 1 month, the growth rate was no different from that of untreated cells. These results indicate that transient treatment with HDAC inhibitor conferred on this cell line a less oncogenic phenotype.

To examine whether the *Brm* gene induced by the HDAC inhibitor treatment is responsible for the antioncogenic potential, PA-1 cells that express short hairpin (sh) RNAs targeting against the *Brm* gene were prepared. For this purpose, we constructed three species of retrovirus vectors (shBrm-1, shBrm-2, and shBrm-4), which target different regions of the *Brm* gene, respectively. At a multiplicity of infection of three for each vector, these three shBrm viruses were introduced into a PA-1 culture. The transduced PA-1 cells did not express Brm protein at all, even after the FK228 treatment, as judged by Western blotting. These cells were treated with FK228 in the same above-mentioned manner, and the tumor invasion assay was performed in the absence of the inhibitors. As shown in Figure 5a, they exhibited an obvious invasion in collagen gel like untreated PA-1 cells. Therefore, we concluded that Brm protein induced by FK228 is directly involved in reducing the oncogenic potential.

We next screened all of the Brm-deficient cell lines listed in Table 1 for the ability to form colonies in soft agar, and found that only SW13(vim-) and NCC-IT cells formed colonies. When both cells were seeded in soft agar 1 day after FK228 treatment, colony formation was observed to be drastically reduced, whereas no significant reduction was observed when HeLa-S3 cells, which are competent for SWI/SNF complex, were treated with FK228 (Figure 5b). These results again support our hypothesis that induction of Brm expression by FK228 reduces the oncogenic potential of Brm-deficient cell lines. Next, we checked the ability to form colonies in soft agar with shBrm-expressing SW13(vim-) cells, but these cells showed reduction in anchorage-independent growth. It was probably because FK228 treatment induce not only Brm but also BRG1 in SW13(vim-) cells (Yamamichi-Nishina *et al*., 2003), and the shBrm virus transduction did not affect the induction of another anti-oncogene, *BRG1*. To produce shBRG1 viruses that knock down the *BRG1* expression, we designed four kinds of shBRG1 virus, but none of them inhibited BRG1 efficiently, and we could not establish the cells in which expression of BRG1 was

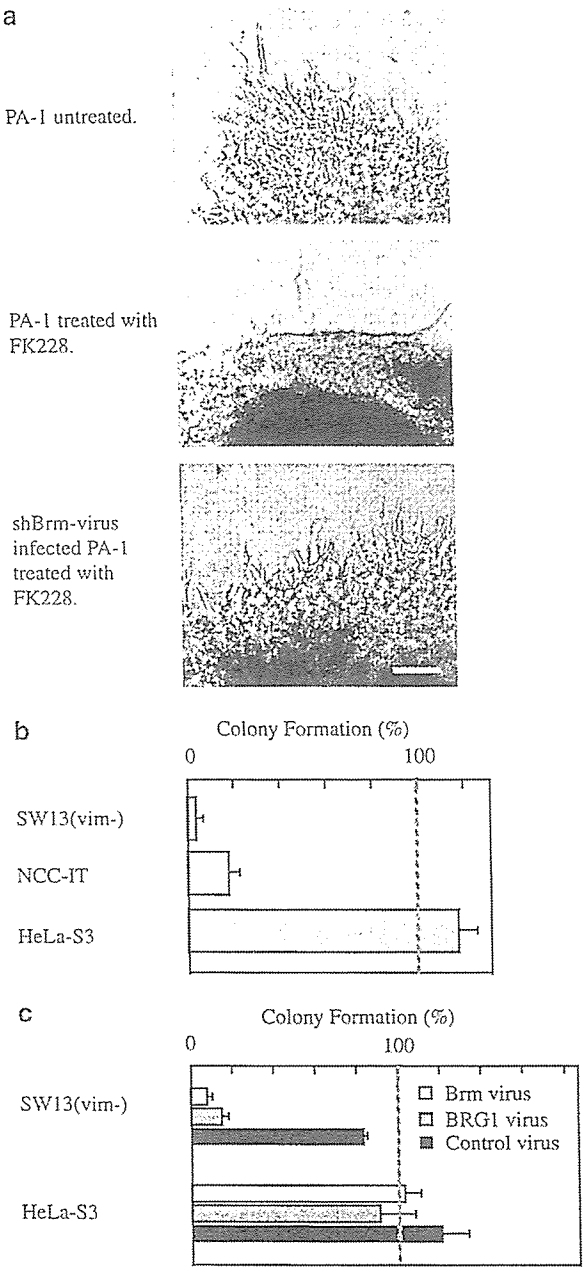

Figure 5 (**a**) 3D collagen gel embedded culture of PA-1 cells. Shown are the peripheral regions of clusters of untreated PA-1 cells (left), PA-1 cells after the FK228 treatment (center), and shBrm-virus-infected PA-1 cells that had been treated with FK228 for 3 days (right). White bar indicates 100 μm. (**b**) Effects of HDAC inhibitor treatment on colony-forming activity in soft agar. SW13(vim-), NCC-IT, and HeLa-S3 cells were treated with FK228 for 3 days at the concentrations shown in Table 2, grown in the absence of FK228 for an additional 24 h, and seeded in soft agar. The number of colonies formed by untreated cells was taken as 100%. The error bar shows the standard deviation based on the results of three experiments. (**c**) Effects of exogenous expression of *Brm* and *BRG1* on colony-forming activity in soft agar. SW13(vim-) and HeLa-S3 cells were infected with Brm-virus, BRG1-virus, or control virus, selected with 1.0 μg/ml puromycin, and seeded in soft agar. The numbers of formed colonies by untreated cells were taken as 100%. The error bar shows the standard deviation based on the results of three experiments

reduced to less than 20% of the parental cell. Making use of shBrm viruses, we were able to prove that Brm expression affects the invasive activity of PA-1 cells, but the relationship between the Brm induction and anchorage-independent growth in SW13(vim-) cells could not be demonstrated.

Exogenous expression of the Brm gene in SW13(vim-) cells suppresses anchorage-independent growth

When the *Brm* gene is introduced into cells that do or do not express endogenous Brm, exogenous expression of Brm protein is strongly attenuated (Bourachot *et al.*, 2003), although the underlying molecular mechanism is still not fully understood. We previously showed that expression of exogenous *Brm* with Brm-virus can attenuate the rapid silencing of retroviral gene transcription in SW13(vim-) and C33A cells by autoregulatory mechanisms, but the stable transductants show only marginal *Brm* expression (Mizutani *et al.*, 2002). Such Brm-virus-infected cells stably retain Brm function, as judged by expression of endogenous genes under the control of AP-1 (Yamamichi-Nishina *et al.*, 2003). These cells also retain the ability to recover from retrovirus gene silencing: the mosaic colony ratio of Brm-virus-infected SW13(vim-) cells was 41%. When such Brm-virus-infected SW13(vim-) cells were assayed for anchorage-independent growth, we found that the colony number of infected cells was much lower than that of control virus-infected cells (Figure 5c). A similar reduction in colony number was observed when BRG1-virus was used. These results indicate that introduction of *Brm* or *BRG1* has an antioncogenic effect on this cell line, which lacks expression of both endogenous BRG1 and Brm. Such reduction in anchorage-independent growth was not observed when HeLa-S3 cells were infected with Brm- or BRG1-virus (Figure 5c).

Discussion

Brm-deficient human cell lines are derived from various types of tumors (Table 1), including embryonic carcinomas and non-small-cell lung carcinomas. We noticed that these cell lines share unique cellular properties. Their cloning by end point dilution was usually difficult, and conditioned medium was needed for the efficient cloning (N Yamamichi and H Iba, unpublished observation). They were often insensitive to conventional assay systems to evaluate oncogenic potential such as colony formation in soft agar. All the Brm-deficient cell lines are examined by the three-dimensional collagen gel embedded culture method, but we detected clear invasive activity only in PA-1 cells (Figure 5a). We could evaluate anchorage-independent growth of SW13(vim-) and NCC-IT cells by colony formation in soft agar (Figure 5b), however, relatively large number of these cells was needed to be seeded for colony formation. Exogenous introduction of the *Brm* gene as well as indirect induction of Brm protein expression by HDAC inhibitors drastically reduced these oncogenic

features, whereas such treatments did not significantly affect the oncogenic potential of human tumor cell lines that have functional SWI/SNF complex. On the basis of these results, we propose that the *Brm* gene has antioncogenic potential. Difficulties in estimating oncogenic potential of Brm-deficient cell lines *in vitro* by conventional methods, however, suggest that it remains to be clarified what kinds of oncogenic parameters are most sensitively affected by the loss of Brm expression. In this regard, it is noteworthy that loss of BRG1/Brm in human lung cancer cell lines and primary lung cancers is reported to correlate with poor prognosis (Reisman *et al*., 2003).

It is interesting that all Brm-deficient cell lines examined here carry a functional *Brm* gene, and Brm deficiency is caused by suppression at the post-transcriptional level. In all of these cell lines, the *Brm* gene was transcribed efficiently, but mature mRNA as well as hnRNA was not detectable. Therefore, the processing of the primary *Brm* transcript to mature mRNA would be affected. We cannot exclude the possibility that *Brm* mRNA transport is also attenuated or that *Brm* mRNA is unstable. For typical tumor suppressor genes, such as *p53*, *Rb*, and *Ini1*, loss of function is usually caused by point mutations in the coding sequence or by deletion of the entire locus (Shimizu *et al*., 1994; Jia *et al*., 1997; Biegel *et al*., 1999). Several other tumor suppressor genes, such as *p16(INK4a)* and *p15(INK4b)*, are often silenced at the level of transcription (Esteller, 2002). Therefore, silencing of the *Brm* gene at the post-transcriptional level is a very unique property among genes with antioncogenic potential. Although molecular mechanisms remain unclear, the post-transcriptional suppression can be attenuated for at least 2 weeks by transient treatment with HDAC inhibitors. This attenuation period is sufficient to either reduce ability of anchorage-independent growth or invasion into collagen gel, thus indicating that HDAC inhibitors may be effective in cancer therapies for Brm-deficient tumor cells. In addition, the HDAC inhibitor-treated cells were shown to be resistant to retroviral gene silencing during this period, suggesting that HDAC inhibitors may be helpful for the cancer gene therapy with retrovirus vectors.

The human SWI/SNF complex utilizes either Brm or BRG1 catalytic subunit to remodel nucleosomes. We found that functional Brm-type SWI/SNF complex, rather than BRG1-type SWI/SNF complex, is directly involved in stable expression of MuLV-based retrovirus probably as a trithorax-G complex, which has been shown to maintain expression of activated genes (Mizutani *et al*., 2002). We also present evidence that Ini1 is an essential subunit for this function; loss of Ini1 yielded the same phenotype of rapid retroviral gene silencing found in Brm-deficient cells. Therefore, we believe that it is unlikely that Brm alone or any other complex containing Brm, but not Ini1, is involved in this function. Consistent with our observation, SNF5, the yeast homologue of Ini1, was reported to be the essential subunit for SWI/SNF complex activity (Geng *et al*., 2001).

When we consider the function of the entire SWI/SNF complex in tumor formation, many questions still remain to be solved. For example, it is not clear whether each SWI/SNF subunit functions to suppress tumor formation as an integral part of the entire complex. Analyses of knockout mice of each subunit of SWI/SNF complex showed that both Ini1 and BRG1 heterozygotes were predisposed to malignant tumors (Bultman *et al*., 2000; Klochendler-Yeivin *et al*., 2000; Barker *et al*., 2001), but phenotypes of the tumors are quite different. It was also reported that SWI/SNF complex formation and the expression of many BRG1-dependent genes are independent of Ini1 expression (Doan *et al*., 2004). It is therefore possible that each of Brm, BRG1, and Ini1 subunits could be a component of other distinct protein complexes that manifest their own tumor-suppressing potential. It is also possible that several additional mutations in other genes would be needed before the loss of SWI/SNF function establish stable neoplastic properties, as the SWI/SNF complex is involved in so many normal cellular functions including transcription, replication, recombination, and cell cycle regulation.

Materials and methods

Cell lines

Human tumor cell lines SW13(vim-) (Yamamichi-Nishina *et al*., 2003), C33A, PA-1, NCC-IT, NCI-H522, A427, H1299, A549, G401, A204, MDA-MB435, SW620, HeLa-S3, and PtG-S2 (prepackaging cell line for retrovirus vector production) were maintained in high glucose DMEM supplemented with 10% fetal calf serum (FCS) (Gibco/Invitrogen Corp., Carlsbad, CA, USA) and incubated at 37°C. EB5 (mouse embryonic stem cell) was maintained at 37°C in GMEM (Sigma) supplemented with 10% FCS, 1% non-essential amino acids (Gibco/Invitrogen Corp.), and leukemia inhibitory factor at 10^3 units/ml. NIH3T3 (mouse fibroblast-like cell) was maintained at 37°C in low glucose DMEM supplemented with 10% calf serum (Gibco/Invitrogen Corp.). When cells were treated with HDAC inhibitors, FK228 (a gift from Fujisawa Corporation, Osaka, Japan) at 0.7–1.6 ng/ml or CHAP31 (a gift from the Japan Energy Corporation, Saitama, Japan) at 5.5 nM were added to the culture medium.

Western blotting

Cells were lysed with 1.5 × sample buffer (91.8 mM Tris-HCl (pH 6.8), 525 mM β-mercaptoethanol, 14.7% glycerol, 3% SDS), and boiled for 10 min at 96°C for denaturation. Whole-cell extracts (20 μg each) were separated by electrophoresis on 6% SDS polyacrylamide gels (for Brm and BRG1) or 10% SDS polyacrylamide gels (for Ini1 and acetylated histone H3), transferred to polyvinylidene difluoride (PVDF) membranes, and immunostained with anti-Brm rabbit polyclonal antibody (Transgenic Inc., Kumamoto, Japan), anti-BRG1 rabbit polyclonal antibody (Santa Cruz Biotechnology, Santa Cruz, CA, USA), anti-BAF47/Ini1 mouse monoclonal antibody (BD Transduction Laboratories, Lexington, KY, USA), or anti-acetylated histone H3 antibody (Upstate Biotechnology, Lake Placid, NY, USA). Specific bands were detected with an ECL kit (Amersham, Piscataway, NJ, USA).

Genomic PCR

Total cellular DNA was prepared using DNA isolation reagent (Wako Pure Chemical Industries, Osaka, Japan). Genomic DNA was amplified using Ex-Taq (Takara Bio Inc., Shiga, Japan) with an initial denaturation at 95°C for 9 min followed by 28 cycles of 95°C for 1 min, 60°C for 1 min, and 72°C for 1 min. The primer pairs were 5′-gttatatgtcaccacacccatc-3′ and 5′-cagatggtctgttgtagttaac-3′ for the fourth exon of *Brm*, and 5′-gtgaacagtcagaaggaagt-3′ and 5′-ttctcatctgaacaggtgat-3′ for the 34th exon (including 3′-noncoding sequence) of *Brm*.

RT–PCR

Total cellular RNA was prepared with Isogen RNA isolation reagent (Wako Pure Chemical Industries, Osaka, Japan), and additionally treated with RQ1 RNase-free DNase (Promega Corp., Madison, WI, USA) to fragment residual genomic DNA completely. Semiquantitative RT–PCR was performed with Superscript One-Step RT–PCR with Platinum Taq Kit (Invitrogen Corp., Carlsbad, CA, USA). In these conditions, we never detected PCR products when the reverse transcription was omitted. The primer pairs to detect *Brm*, *BRG1*, and *Ini1* mRNAs were 5′-ctgcaagagcgggaatacagacttcaggcccg-3′ and 5′-ggctgcctgggcttgcttgtgctcccaaacc-3′ for the 5′-region of *Brm*, 5′-agaaggtgcccagtaattctcagttgg-3′ and 5′- actcactgggta gaaatgagacaggggagg-3′ for the 3′-region of *Brm*, 5′-ctggccc ttcccctggagccatgct-3′ and 5′-agggccgggtcctgttgcggacac-3′ for *BRG1*, and 5′-acctacctcagggagcagaaggccaagagg-3′ and 5′-cagc ttcagggcaaacttctctgg-3′ for *Ini1*. The primer pairs to detect *Brm* hnRNAs were 5′-tatctctctttcagggttgtc-3′ (locating in third intron) and 5′-cagatggtctgttgtagttaac-3′ (locating in fourth exon) for the 5′-region of *Brm*, and 5′-gaattatgatctcaccc cagcctt-3′ (locating in 32nd intron) and 5′-actcactgggtagaaat gagacaggggagg-3′ (locating in 33rd exon) for the 3′-region of *Brm*. RNA was reverse transcribed for 30 min at 50°C, and for *Brm* and *BRG1* mRNA, cDNA was amplified with an initial denaturation at 94°C for 3 min followed by 30 cycles of 94°C for 30 s, 66°C for 2 min, and 72°C for 1 min. For *Ini1* mRNA, cDNA was amplified with an initial denaturation at 94°C for 3 min followed by 30 cycles of 94°C for 30 s, 62°C for 1 min, and 72°C for 1 min. For *Brm* hnRNA, cDNA was amplified with an initial denaturation at 94°C for 3 min followed by 35 or 40 cycles of 94°C for 30 s, 58°C for 1 min, and 72°C for 1 min.

Nuclear run-on transcription assay

Nuclei were isolated from $2x10^7$ cells of each cell line. Transcript elongation assay was performed as described previously (Yamamichi-Nishina *et al*., 2003), and RNA labeled with [α-^{32}P]UTP was isolated from each sample. All samples had very close total radioactivity and were hybridized to Hybond N$^+$ filters that were slot-blotted with several plasmid DNAs (5 μg) including pBluescriptSK(+)-Brm, pBluescriptSK(+)-BRG1, pCR2.1-Brm(F), pBluescript SK(+)-Brm(G), pBluescriptSK(+)-Brm(H), pBluescript SK(+)-CD44, pCR2.1-collagenase, and pCR2.1-β-actin. As a control, pCR2.1 or pBluescriptSK(+) was also slot-blotted. Construction of these plasmids was described previously (Yamamichi-Nishina *et al*., 2003).

Retrovirus vectors

Vesicular stomatitis virus G protein (VSV-G)-pseudotyped, MuLV-based replication-defective retrovirus vectors were prepared with prepackaging cell line PtG-S2 (Arai *et al*., 1998) or prepackaging cell line PLAT (Morita *et al*., 2000). Brm-virus, BRG1-virus, and control virus were produced by introducing pBabe-hBrm-IRESpuro, pBabe-hBRG1-IRESpuro, and pBabe-IRESpuro, respectively, into PtG-S2 cells (Mizutani *et al*., 2002). MFGnlsLacZ, which encodes LacZ with a nuclear localization signal, was used as the LacZ virus (Ui *et al*., 2000). To produce a retroviral vector expressing short hairpin RNA (shRNA) to inhibit *Brm* expression, oligonucleotides 5′-ctagcggatccatgagaattcg-3′ and 5′-tcgacgaattctcatggatccg-3′ were inserted into the *Nhe*I–*Sal*I site of modified pQCXIH vector (Clontech, Palo Alto, CA, USA), so as to generate *Bam*HI and *Eco*RI restriction sites in the U3 region located in 3′-long terminal repeat. Next, CMV promoter-IRES-hygromycin of the pQCXIH-based plasmid was replaced by the fragment carrying SV40 promoter-puromycin from pBabe-puro plasmid (Ui *et al*., 2000) to generate a retroviral vector designated as pSSSP (pSIN-siRNA-SV40puro). pmU6 was constructed as reported previously (Yu *et al*., 2002), and to produce the pmU6-shRNA cassette, each of following oligonucleotide pairs were annealed and inserted into the *Bbs*I–*Eco*RI site of pmU6: shBrm-1 corresponding to nt 2998–3018 of *Brm* coding region, shBrm-2 corresponding to nt 225–245 of *Brm* coding region, and shBrm-4 corresponding to nt 5425-5445 of *Brm* coding and noncoding region. *Bam*HI–*Eco*RI fragments of each pmU6-shRNA cassette were subcloned into the *Bam*HI-*Eco*RI site of pSSSP. Three types of shBrm virus were produced by introducing pSSSP-shBrm-1, pSSSP-shBrm-2, and pSSSP-shBrm-4 into PLAT cells (Morita *et al*., 2000) with the plasmid coding VSV-G (Arai *et al*., 1998).

Mosaic colony assay

All the cell lines were transduced with LacZ virus at a low multiplicity of infection (about 0.1–0.5) to minimize introduction of multiple proviral copies into a single cell. To complete the retroviral integration, the transduced cells were grown for 24 h and seeded at very low density for isolation of individual colonies. Cells were grown for an additional 72 h to form colonies consisting of 6–20 cells. These colonies were fixed and stained with colorant solution (5 mM $K_3Fe(CN)_6$, 5 mM $K_4[Fe(CN)_6]\cdot 3H_2O$, 2 mM $MgCl_2$, 1 mg/ml X-gal) to examine LacZ expression. Formed colonies were classified into three types: 'positive', in which all cells express LacZ; 'negative', in which no cells express LacZ; and 'mosaic', which contain both LacZ-positive and LacZ-negative cells. The 'mosaic colony ratio' was calculated as the number of mosaic colonies divided by the sum of the number of positive colonies and the number of mosaic colonies.

Tumor invasion assay (3D collagen gel embedded culture method)

To prepare collagen gels for tumor invasion assay, Cellmatrix Type I-A Collagen Kit (Nitta Gelatin Inc., Osaka, Japan) was used. Type I-A collagen was mixed with 5 × DMEM and sterile constitution buffer (2.2 g $NaHCO_3$ in 100 ml 0.05 N NaOH/200 mM HEPES) at a 7 : 2 : 1 ratio on ice. Reconstituted collagen solution (200 μl) was added to a 24-well plate to make the bottom collagen gel layer and maintained at 37°C for 30 min until solid. Fresh reconstituted collagen solution (600 μl) was poured onto the solidified bottom layer, and the culture plate was incubated at 37°C for an additional 6 min. Cells (5×10^3) suspended in 5 μl of culture medium were then injected into the center of this top layer. The culture plate was incubated at 37°C for 25 min to complete solidification. Finally, 400 μl of culture medium was poured onto these gel layers, and the cells embedded in the top layer were grown for 7–12 days at 37°C.

Colony formation in soft agar

SW13(vim-), NCC-IT, and HeLa-S3 cells were seeded into 60-mm dishes as a suspension of 0.4%. Noble agar (BD Company, Sparks, MD, USA) in high glucose DMEM supplemented with 10% FCS and 0.5 μg/ml amphotericin B (Sigma). The upper agar layers were on top of beds of 0.5% Bacto agar (BD Company) in high glucose DMEM supplemented with 10% FCS and 5.0 μg/ml amphotericin B (bottom agar layers). Cultures were incubated at 37°C for 28 days, and the resulting colonies were counted. The average of three experiments is shown with standard deviation.

Acknowledgements

We thank Japan Energy Corporation and Fujisawa Corporation for supplying CHAP31 and FK228, respectively. Anti-Brm antibody was supplied by Kumamoto Immunochemical Laboratory, Transgenic Inc., Kumamoto, Japan. We thank Drs Yana and Seiki (Division of Cancer Cell Research, Institute of Medical Science, University of Tokyo) for technical advice regarding the tumor invasion assay, Drs Kameda and Sugiyama (Department of Biochemistry, Akita University School of Medicine) for useful suggestion in producing pSSSP vector, Dr Kitamura (Division of Cellular Therapy, Institute of Medical Science, University of Tokyo) for providing us the PLAT packaging cell line, and Dr Yoshida for fruitful discussion concerning HDAC inhibitors. SW13 and G401 were obtained from Japanese Collection of Research Bioresources, and PA-1 and A549 were obtained from Cell Resource Center for Biomedical Research, Tohoku University. We were also grateful to Dr Niwa (Riken Center) for his gift of EB5 (embryonic stem cell), and also grateful to N Hashimoto and K Takeda for assistance in preparing this paper. This work was supported in part by a Grant-in-Aid for Scientific Research on Priority Areas from the Ministry of Education, Cultures, Sports, Science, and Technology of Japan.

References

Arai T, Matsumoto K, Saitoh K, Ui M, Ito T, Murakami M, Kanegae Y, Saito I, Cosset FL, Takeuchi Y and Iba H. (1998). *J. Virol.*, **72**, 1115–1121.

Barker N, Hurlstone A, Musisi H, Miles A, Bienz M and Clevers H. (2001). *EMBO J.*, **20**, 4935–4943.

Betz BL, Strobeck MW, Reisman DN, Knudsen ES and Weissman BE. (2002). *Oncogene*, **21**, 5193–5203.

Biegel JA, Zhou JY, Rorke LB, Stenstrom C, Wainwright LM and Fogelgren B. (1999). *Cancer Res.*, **59**, 74–79.

Bourachot B, Yaniv M and Muchardt C. (2003). *EMBO J.*, **22**, 6505–6515.

Bultman S, Gebuhr T, Yee D, La Mantia C, Nicholson J, Gilliam A, Randazzo F, Metzger D, Chambon P, Crabtree G and Magnuson T. (2000). *Mol. Cell.*, **6**, 1287–1295.

Cheng SW, Davies KP, Yung E, Beltran RJ, Yu J and Kalpana GV. (1999). *Nat. Genet.*, **22**, 102–105.

DeCristofaro MF, Betz BL, Rorie CJ, Reisman DN, Wang W and Weissman BE. (2001). *J. Cell. Physiol.*, **186**, 136–145.

DeCristofaro MF, Betz BL, Wang W and Weissman BE. (1999). *Oncogene*, **18**, 7559–7565.

Doan DN, Veal TM, Yan Z, Wang W, Jones SN and Imbalzano AN. (2004). *Oncogene*, **23**, 3462–3473.

Dunaief JL, Strober BE, Guha S, Khavari PA, Alin K, Luban J, Begemann M, Crabtree GR and Goff SP. (1994). *Cell*, **79**, 119–130.

Esteller M. (2002). *Oncogene*, **21**, 5427–5440.

Furumai R, Matsuyama A, Kobashi N, Lee KH, Nishiyama M, Nakajima H, Tanaka A, Komatsu Y, Nishino N, Yoshida M and Horinouchi S. (2002). *Cancer Res.*, **62**, 4916–4921.

Geng F, Cao Y and Laurent BC. (2001). *Mol. Cell. Biol.*, **21**, 4311–4320.

Guidi CJ, Sands AT, Zambrowicz BP, Turner TK, Demers DA, Webster W, Smith TW, Imbalzano AN and Jones SN. (2001). *Mol. Cell. Biol.*, **21**, 3598–3603.

Iba H, Mizutani T and Ito T. (2003). *Rev. Med. Virol.*, **13**, 99–110.

Ito T, Yamauchi M, Nishina M, Yamamichi N, Mizutani T, Ui M, Murakami M and Iba H. (2001). *J. Biol. Chem.*, **276**, 2852–2857.

Jia LQ, Osada M, Ishioka C, Gamo M, Ikawa S, Suzuki T, Shimodaira H, Niitani T, Kudo T, Akiyama M, Kimura N, Matsuo M, Mizusawa H, Tanaka N, Koyama H, Namba M, Kanamaru R and Kuroki T. (1997). *Mol. Carcinogen.*, **19**, 243–253.

Klochendler-Yeivin A, Fiette L, Barra J, Muchardt C, Babinet C and Yaniv M. (2000). *EMBO Rep.*, **1**, 500–506.

Komatsu Y, Tomizaki KY, Tsukamoto M, Kato T, Nishino N, Sato S, Yamori T, Tsuruo T, Furumai R, Yoshida M, Horinouchi S and Hayashi H. (2001). *Cancer Res.*, **61**, 4459–4466.

Laurent BC, Treich I and Carlson M. (1993). *Genes Dev.*, **7**, 583–591.

Lee D, Kim JW, Seo T, Hwang SG, Choi EJ and Choe J. (2002). *J. Biol. Chem.*, **277**, 22330–22337.

LeGouy E, Tompson EM, Muchardt C and Renard J-P. (1998). *Dev. Dyn.*, **212**, 38–48.

Mizutani T, Ito T, Nishina M, Yamamichi N, Watanabe A and Iba H. (2002). *J. Biol. Chem.*, **277**, 15859–15864.

Morita S, Kojima T and Kitamura T. (2000). *Gene Therapy*, **7**, 1063–1066.

Nakajima H, Kim YB, Terano H, Yoshida M and Horinouchi S. (1998). *Exp. Cell. Res.*, **241**, 126–133.

Narlikar GJ, Fan HY and Kingston RE. (2002). *Cell*, **108**, 475–487.

Reisman DN, Sciarrotta J, Wang W, Funkhouser WK and Weissman BE. (2003). *Cancer Res.*, **63**, 560–566.

Reisman DN, Strobeck MW, Betz BL, Sciariotta J, Funkhouser Jr W, Murchardt C, Yaniv M, Sherman LS, Knudsen ES and Weissman BE. (2002). *Oncogene*, **21**, 1196–1207.

Reyes JC, Barra J, Muchardt C, Camus A, Babinet C and Yaniv M. (1998). *EMBO J.*, **17**, 6979–6991.

Roberts CW, Galusha SA, McMenamin ME, Fletcher CD and Orkin SH. (2000). *Proc. Natl. Acad. Sci. USA*, **97**, 13796–13800.

Shimizu E, Coxon A, Otterson GA, Steinberg SM, Kratzke RA, Kim YW, Fedorko J, Oie H, Johnson BE, Mulshine JL, Minna JD, Gazdar AF and Kaye FJ. (1994). *Oncogene*, **9**, 2441–2448.

Strobeck MW, Knudsen KE, Fribourg AF, DeCristofaro MF, Weissman BE, Imbalzano AN and Knudsen ES. (2000). *Proc. Natl. Acad. Sci. USA*, **97**, 7748–7753.

Trouche D, Le Chalony C, Muchardt C, Yaniv M and Kouzarides T. (1997). *Proc. Natl. Acad. Sci. USA*, **94,** 11268–11273.

Ui M, Mizutani T, Takada M, Arai T, Ito T, Murakami M, Koike C, Watanabe T, Yoshimatsu K and Iba H. (2000). *Biochem. Biophys. Res. Commun.*, **278,** 97–105.

Versteege I, Sevenet N, Lange J, Rousseau-Merck MF, Ambros P, Handgretinger R, Aurias A and Delattre O. (1998). *Nature*, **394,** 203–206.

Wang W, Xue Y, Zhou S, Kuo A, Cairns BR and Crabtree GR. (1996). *Genes Dev.*, **10,** 2117–2130.

Wong AK, Shanahan F, Chen Y, Lian L, Ha P, Hendricks K, Ghaffari S, Iliev D, Penn B, Woodland AM, Smith R, Salada G, Carillo A, Laity K, Gupte J, Swedlund B, Tavtigian SV, Teng DH and Lees E. (2000). *Cancer Res.*, **60,** 6171–6177.

Yamamichi-Nishina M, Ito T, Mizutani T, Yamamichi N, Watanabe H and Iba H. (2003). *J. Biol. Chem.*, **278,** 7422–7430.

Yu JY, DeRuiter SL and Turner DL. (2002). *Proc. Natl. Acad. Sci. USA*, **99,** 6047–6052.

Contrast-Enhanced Ultrasonography in the Diagnosis of Solid Renal Tumors

Hideyuki Tamai, MD, Yoshie Takiguchi, MT, Masashi Oka, MD, Naoki Shingaki, MD, Shotaro Enomoto, MD, Tatsuya Shiraki, MD, Machi Furuta, MD, Izumi Inoue, MD, Mikitaka Iguchi, MD, Kimihiko Yanaoka, MD, Kenji Arii, MD, Yasuhito Shimizu, MD, Hiroya Nakata, MD, Toshiaki Shinka, MD, Tokio Sanke, MD, Masao Ichinose, MD

Objective. The purpose of this study was to evaluate the usefulness of contrast-enhanced ultrasonography (CEUS) in the diagnosis of solid renal tumors. ***Methods.*** Twenty-nine patients with solid tumors detected on gray scale ultrasonography underwent resection for suspected renal malignancy. Findings of arterial phase contrast computed tomography (CT) and CEUS were compared for each diagnosis. ***Results.*** Histopathologic examination of resected lesions showed malignancy in 26 patients (clear cell carcinoma, n = 18; papillary renal cell carcinoma, n = 6; collecting duct carcinoma, n = 1; and infiltrative urothelial carcinoma, n = 1) and benign tumors in 3 patients (oncocytoma, n = 2; and angiomyolipoma, n = 1). Contrast CT failed to show tumor blood flow in 5 of 29 patients, whereas CEUS showed this in all patients. Positive predictive values of CEUS and contrast CT in the diagnosis of renal malignancy were 100% and 82.8%, respectively. Among clear cell carcinomas, hypervascularity was observed on contrast CT in 16 of 18 patients and on CEUS in 17 of 18 patients. On the basis of hypervascularity, diagnostic sensitivity values for clear cell carcinoma were 94.4% for CEUS and 88.9% for contrast CT, whereas specificity values were 45.5% for CEUS and 72.7% for contrast CT. Among papillary cell carcinomas, contrast CT showed avascular lesions in 4 of 6 patients. However, CEUS showed blood flow in these lesions, leading to diagnosis of hypovascular renal tumors. ***Conclusions.*** Contrast-enhanced ultrasonography was more sensitive for detecting slight tumor blood flow than contrast CT and was useful in preoperatively diagnosing malignant hypovascular renal tumors but was less so for hypervascular renal tumors. ***Key words:*** clear cell carcinoma; contrast computed tomography; contrast-enhanced ultrasonography; renal tumor.

Abbreviations
CEUS, contrast-enhanced ultrasonography; CT, computed tomography; MRI, magnetic resonance imaging

Received April 20, 2005, from the Second Department of Internal Medicine (H.T., M.O., N.S., Ta.S., I.I., M.I., K.Y., K.A., Y.S., H.N., M.I.) and Department of Urology (Tos.S.), Wakayama Medical University, Wakayama, Japan; and Laboratory Center, Wakayama Medical University Hospital, Wakayama, Japan (Y.T., M.F., Tok.S.). Revision requested June 13, 2005. Revised manuscript accepted for publication July 13, 2005.

Address correspondence to Hideyuki Tamai, MD, Second Department of Internal Medicine, Wakayama Medical University, 811-1 Kimiidera, Wakayama City, Wakayama 640-0012, Japan.
E-mail: tamahide@wakayama-med.ac.jp

Imaging studies used to evaluate renal lesions include ultrasonography, computed tomography (CT), and magnetic resonance imaging (MRI). Of these modalities, ultrasonography is the easiest to perform and the least invasive. In Japan, the use of ultrasonography in mass screening has increased the number of incidentally discovered asymptomatic renal cell carcinomas.[1]

When solid renal masses are detected on conventional ultrasonography, it is important to differentiate between benign and malignant tumors. Benign solid masses that should be differentiated from renal cell carcinoma are angiomyolipoma, lipoma, adenoma, oncocytoma, and pseudotumors such as the hypertrophied column of Bertin and fetal lobulation. Diagnosis of angiomyolipoma or lipoma is relatively easy if the fat component of the

 • J Ultrasound Med 2005; 24:1635–1640 • 0278-4297/05/$3.50

tumor is shown on MRI or CT. Otherwise, however, it is difficult to ascertain whether the lesion is malignant; this frequently requires fine-needle biopsy, a technique that carries an inherent risk of tumor cell seeding.

Renal cell carcinoma is characterized by rich blood flow, and, in general, arterial hypervascularity on contrast imaging is clinically regarded as evidence of this tumor. Information on blood flow is therefore essential in diagnosing renal lesions and planning treatment. If blood flow is not detected within a solid tumor, although it can be useful to perform invasive studies such as angiography or tumor biopsy, many of these lesions are followed without surgery. Currently, contrast CT is most often used to evaluate renal tumor blood flow. This modality is more sensitive than ultrasonography in detecting a tumor thrombus in the renal vein and inferior vena cava or metastasis and invasion of adjacent organs and is therefore used to decide tumor staging for surgical treatment.[2] However, disadvantages of contrast CT include radiation exposure, the risk of inducing severe renal dysfunction, and contraindication in patients allergic to iodine. Conversely, contrast-enhanced ultrasonography (CEUS) is more sensitive than color Doppler ultrasonography in detecting blood flow, involves no radiation exposure, and can be performed safely when contrast CT is contraindicated. Although potentially a very useful imaging tool, CEUS is still not widely used in clinical practice, and few reports have discussed its use in the evaluation of renal tumors.[3,4] In this study, we evaluated and compared the usefulness of CEUS with contrast CT in the diagnosis of renal tumors.

Materials and Methods

The subjects were 29 patients in whom solid renal tumors were detected on conventional gray scale ultrasonography. All underwent further evaluation with contrast CT and CEUS, and tumors suspected to be malignant were resected at the Department of Urology of our university hospital between March 2002 and October 2004. The final pathologic diagnosis of the solid renal tumors was confirmed from resected kidneys. Informed consent was obtained from all patients. Twenty-one men and 8 women were enrolled, with a mean age ± SD of 63.5 ± 11.9 years. The mean tumor diameter was 51.3 ± 20.8 mm.

Contrast-enhanced ultrasonography was performed with a Sonoline Elegra system (Siemens Medical Solutions, Erlangen, Germany) using the Sie Flow mode and a 2.5-g intravenous bolus of Levovist (SH U 508A; Schering AG, Berlin, Germany) as a contrast agent. The following ultrasound settings were used: transmission frequency of 2.8 MHz, maximum output of 100%, single-point focus (center or lower margin of tumor), and frame rate of 5 per second. The contrast agent was injected, and while patients held their breath after the contrast appeared on imaging, the frame rate was gradually decreased from 5 to 2 and then to 1 per second, and arterial phase imaging was performed.

Computed tomography was performed with an Aquilion multidetector-row CT scanner (Toshiba Medical Systems Co, Ltd, Tochigi, Japan) at 120 kV (peak) and a revolution time of 0.5 seconds. Using a mechanical injector, 100 mL of nonionic contrast media (iopamidol 300; Bracco SpA, Milan, Italy) was injected into a peripheral vein at a rate of 3.0 mL/s. A reconstruction interval of 5 mm was chosen for all studies. Scanning of the arterial phase was started 30 seconds after contrast agent injection. Tumor blood flow on contrast was evaluated on CT and CEUS by comparing the degree of arterial phase tumor staining with that of renal cortical staining. Because the kidney is a highly vascular organ, tumor blood flow equal to or greater than cortical blood flow was defined as hypervascular, tumor blood flow less than cortical blood flow as hypovascular, and absence of tumor blood flow as avascular. Contrast-enhanced ultrasonographic studies were reviewed by an internist, and contrast CT studies were reviewed by a radiologist. For each histopathologic diagnosis confirmed from resected lesions, CEUS and contrast CT findings were compared.

Results

Histopathologic examination of the resected lesions showed malignant tumors in 26 patients (clear cell carcinoma, n = 18; papillary renal cell carcinoma, n = 6; collecting duct carcinoma, n = 1; and infiltrative urothelial carcinoma, n = 1). Three patients had benign tumors (oncocytoma, n = 2; and angiomyolipoma, n = 1). Contrast CT failed to show tumor blood flow in 5 of 29 patients, whereas CEUS showed tumor blood flow in all patients. Positive predictive values for

CEUS and contrast CT in the diagnosis of renal tumor were 100% and 82.8%, respectively. Hence, CEUS was more sensitive in detecting tumor blood flow.

Evaluation of tumor blood flow by CEUS and contrast CT for each histopathologic diagnosis is summarized in Tables 1 and 2. The findings of arterial phase contrast CT and CEUS were compared for each histopathologic diagnosis. Among clear cell carcinomas, hypervascularity was shown on contrast CT in 16 of 18 patients and on CEUS in 17 of 18 patients. On the basis of hypervascularity, diagnostic sensitivity and specificity for clear cell carcinoma were 94.4% and 45.5%, respectively, for CEUS versus 88.9% and 72.7% for contrast CT. Contrast-enhanced ultrasonography therefore had better sensitivity but worse specificity than contrast CT. Among papillary cell carcinomas, contrast CT showed avascular lesions in 4 of 6 patients. The radiologist diagnosed hemorrhagic simple cysts in these cases; however, CEUS showed blood flow in these lesions, indicating hypovascular renal tumors (Figure 1).

For the collecting duct carcinoma, contrast CT showed an avascular lesion, whereas CEUS showed slight blood flow consistent with a hypovascular renal tumor (Figure 2). For the infiltrative urothelial carcinoma, contrast CT showed hypovascularity, but CEUS showed hypervascularity. Hence, CEUS was more sensitive in detecting blood flow in this tumor. In the 2 oncocytomas, both contrast CT and CEUS showed hypervascular lesions, making them difficult to distinguish from renal cell carcinomas on the basis of blood flow alone. In 1 patient, however, CEUS depicted tumor vessels in a spoke wheel configuration, leading to a preoperative diagnosis of oncocytoma (Figure 3). In the angiomyolipoma, contrast CT showed hypovascularity, whereas CEUS showed hypervascularity. Magnetic resonance imaging showed very few fatty elements, making it difficult to preoperatively distinguish the angiomyolipoma from renal cell carcinoma.

Discussion

In solid renal tumors detected by gray scale ultrasonography, differentiation between malignant and benign lesions is essential. Although non–contrast-enhanced ultrasonography is good at detecting renal tumors, it is difficult to characterize the tumor lesion with this modality. Evaluation of tumor vascularity is particularly important in tumor characterization. If slight blood flow is shown within the tumor by any contrast modality, the possibility of malignancy is raised.

Clear cell carcinoma accounts for about 70% of renal carcinoma and is easy to diagnose from its typical angiographic appearance of hypervascularity, as evidenced by strong contrast enhancement.[5] Conversely, hypovascular renal cell carcinoma, with weak or absent contrast enhancement, tends to be difficult to diagnose preoperatively. Such renal tumors, some of which have a poor prognosis, include papillary renal cell carcinoma, chromophobe cell carcinoma, cystic renal cell carcinoma, clear cell sarcoma, spindle cell carcinoma, and collecting duct carcinoma.[6] Even slight blood flow on contrast studies of these lesions can lead clinicians to suspect a hypovascular tumor and consider surgical treatment. However, if no blood flow is detected, it is difficult to determine whether these lesions are benign or malignant. Options in such patients include angiography, which is an invasive procedure, renal biopsy, which is associated with a risk of tumor seeding, and careful follow-up observation.

This study showed no marked difference between contrast CT and CEUS in the ability to diagnose clear cell carcinoma; the sensitivity of

Table 1. Evaluation of Blood Flow by Contrast-Enhanced Computed Tomography for Each Histopathologic Diagnosis

Diagnosis	n	Hypervascular	Hypovascular	Avascular
Clear cell carcinoma	18	16	2	0
Papillary renal cell carcinoma	6	0	2	4
Collecting duct carcinoma	1	0	0	1
Infiltrative urothelial carcinoma	1	0	1	0
Oncocytoma	2	2	0	0
Angiomyolipoma	1	0	1	0

Table 2. Evaluation of Blood Flow by CEUS for Each Histopathologic Diagnosis

Diagnosis	n	Hypervascular	Hypovascular	Avascular
Clear cell carcinoma	18	17	1	0
Papillary renal cell carcinoma	6	2	4	0
Collecting duct carcinoma	1	0	1	0
Infiltrative urothelial carcinoma	1	1	0	0
Oncocytoma	2	2	0	0
Angiomyolipoma	1	1	0	0

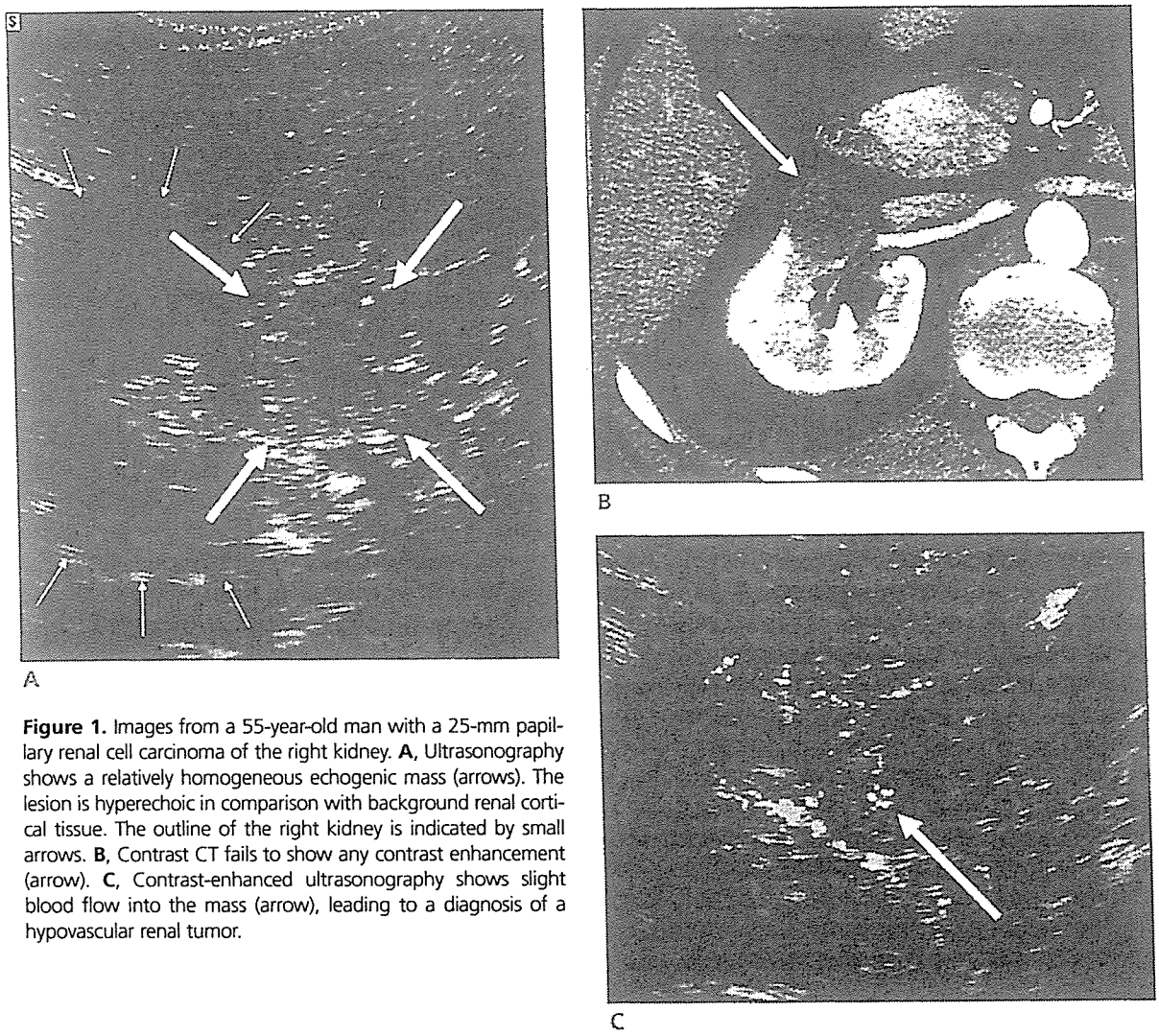

Figure 1. Images from a 55-year-old man with a 25-mm papillary renal cell carcinoma of the right kidney. **A**, Ultrasonography shows a relatively homogeneous echogenic mass (arrows). The lesion is hyperechoic in comparison with background renal cortical tissue. The outline of the right kidney is indicated by small arrows. **B**, Contrast CT fails to show any contrast enhancement (arrow). **C**, Contrast-enhanced ultrasonography shows slight blood flow into the mass (arrow), leading to a diagnosis of a hypovascular renal tumor.

both methods was approximately 90%. Contrast CT is better than ultrasonography in evaluating extracapsular spread and lymph node metastases,[7] and in cases in which renal cell carcinoma is diagnosed by contrast CT, further evaluation with CEUS is generally thought to be unnecessary. Moreover, the specificity of CEUS was not particularly higher than that of contrast CT. Because some hypovascular tumors diagnosed by contrast CT were hypervascular on CEUS, differentiation from clear cell carcinoma could not be made from the CEUS findings in these cases.

Angiomyolipoma is a benign tumor that is easy to diagnose when CT and MRI show fatty elements. The angiomyolipoma in this study, however, had a small fatty component, making it difficult to distinguish from renal cell carcinoma.[8] Contrast-enhanced ultrasonography was not helpful in this particular case. Oncocytoma is a benign tumor with rich blood flow, and although differential diagnosis from renal cell carcinoma can be difficult, a spoke wheel configuration of nutrient vessels is characteristic.[9] In 1 of our 2 patients with oncocytoma, CEUS depicted this configuration, leading to the type of neoplasm being diagnosed preoperatively. Contrast-enhanced ultrasonography can visualize vascular structures in real time from any arbitrary section, and depiction of a spokelike configuration can be useful in the diagnosis of oncocytoma.

In this study, CEUS was more sensitive than contrast CT in detecting hypovascular renal tumors. In all 5 patients in whom contrast CT failed to show blood flow, CEUS was able to depict flow, thereby proving useful in diagnosing hypovascular tumors. Contrast-enhanced ultrasonography was most useful in such patients in diagnosis and planning treatment; without

Figure 2. Images from a 53-year-old man with a 20-mm collecting duct carcinoma of the right kidney. **A**, Ultrasonography shows a hyperechoic mass and hypoechoic halo (arrows). **B**, Contrast CT fails to show any contrast enhancement (arrow). **C**, Contrast-enhanced ultrasonography shows small microbubbles in the mass (arrow), leading to a diagnosis of a hypovascular renal tumor.

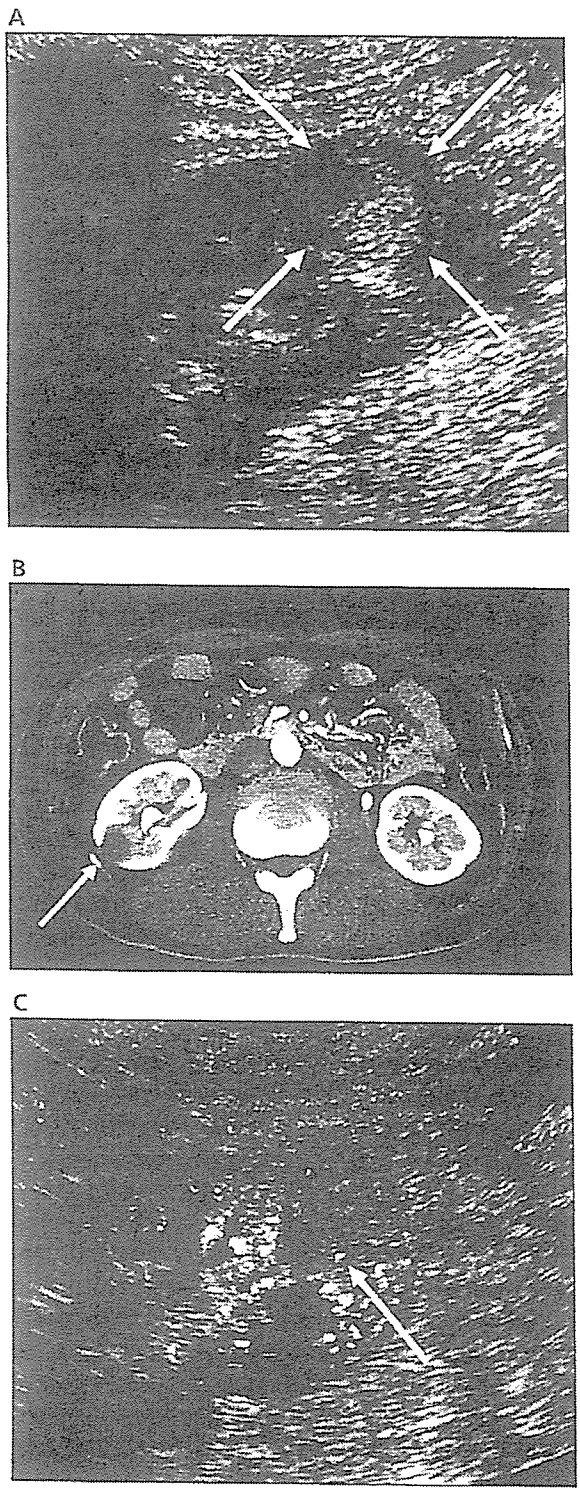

CEUS in these patients, the renal tumor would not be characterized, and further options would involve renal biopsy or careful follow-up monitoring. Furthermore, CEUS showed high specificity in that all patients with demonstrable blood flow had malignant renal tumors. Our findings show that CEUS provides useful information in diagnosing and planning treatment of hypovascular renal tumors. We therefore recommend that CEUS should be performed in the differential diagnosis of renal lesions if contrast CT fails to show blood flow.

Figure 3. Images from a 53-year-old man with a 60-mm oncocytoma of the left kidney. **A**, Computed tomography during angiography shows a rich tumor blood supply but does not show a definite spoke wheel configuration (arrow). This makes it difficult to distinguish the tumor from clear cell carcinoma. **B**, Contrast-enhanced ultrasonography shows tumor vessels in a spoke wheel configuration.

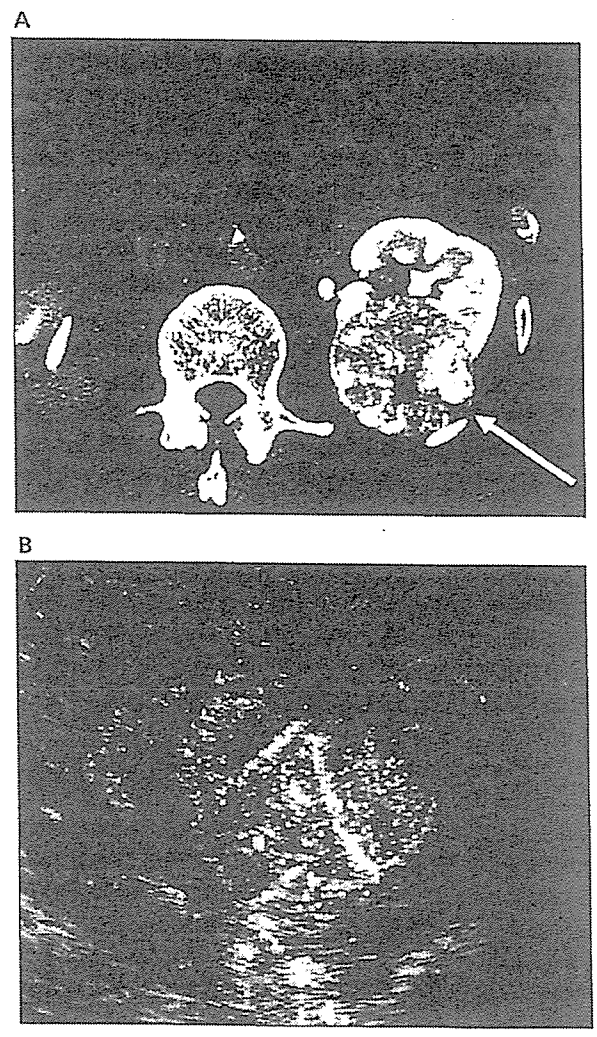

The patients in this study all had solid renal tumors on ultrasonography. In patients with complicated and problematic cystic lesions, differentiating between benign and malignant lesions is difficult, although further examinations, including Doppler ultrasonography, contrast CT, and MRI, have been performed. Kim et al[3] reported a preliminary study of contrast-enhanced power Doppler ultrasonography for the differentiation of cystic renal lesions for this purpose. Moreover, Robbin et al[10] mentioned that CEUS might replace CT in the evaluation and follow-up of complex renal cysts, eliminating the need for costly CT scans with their attendant potential contrast agent nephrotoxicity. Further large studies of CEUS in cystic renal lesions is required.

In conclusion, in the evaluation of solid renal lesions, CEUS is less invasive than contrast CT and can show even slight tumor blood flow. This imaging technique shows both tumor staining and vascular structures in detail and may be useful in patients in whom contrast CT or contrast MRI is contraindicated. In addition, CEUS is more useful in diagnosing hypovascular renal tumors than in diagnosing hypervascular renal tumors such as clear cell carcinoma.

References

1. Mihara S, Kuroda K, Yoshioka R, Koyama W. Early detection of renal cell carcinoma by ultrasonographic screening: based on the results of 13 years screening in Japan. Ultrasound Med Biol 1999; 25:1033–1039.
2. Kopka L, Fisher U, Zoeller G, Schmidt C, Ringert RH, Grabbe E. Dual-phase helical CT of the kidney: value of the corticomedullary and nephrographic phase for evaluation of renal lesions and preoperative staging of renal cell carcinoma. AJR Am J Roentgenol 1997; 169:1573–1578.
3. Kim AY, Kim SH, Kim YJ, Lee IH. Contrast-enhanced power Doppler sonography for the differentiation of cystic renal lesions: preliminary study. J Ultrasound Med 1999; 18:581–588.
4. Reichelt O, Wunderlich H, Weirich T, Schlichter A, Schubert J. Computerized contrast angiography: a new diagnostic tool for the urologist? BJU Int 2001; 88:9–14.
5. Bostwick DG, Eble JN. Diagnosis and classification of renal cell carcinoma. Urol Clin North Am 1999; 26:627–635.
6. Onishi T, Oishi Y, Goto H, Yanada S, Abe K. Histological features of hypovascular or avascular renal cell carcinoma: the experience at four university hospitals. Int J Clin Oncol 2002; 7:159–164.
7. Reznek RH. Imaging in the staging of renal cell carcinoma. Eur Radiol 1996; 6:120–128.
8. Hosokawa Y, Kinouchi T, Sawai Y, et al. Renal angiomyolipoma with minimal fat. Int J Clin Oncol 2002; 7:120–123.
9. Quinn MJ, Hartman DS, Friedman AC, et al. Renal oncocytoma: new observations. Radiology 1984; 153:49–53.
10. Robbin ML, Lockhart ME, Barr RG. Renal imaging with ultrasound contrast: current status. Radiol Clin North Am 2003; 41:963–978.

Develop. Growth Differ. (2005) **47**, 573–580

Endothelin-3 controls growth of colonic epithelial cells by mediating epithelial–mesenchymal interaction

Hiroshi Fukamachi,[1,*] Takanori Narita,[1] Naohisa Yahagi,[2] Hiroyuki Takeda[1] and Masao Ichinose[3]

[1]*Department of Biological Sciences, Graduate School of Science, University of Tokyo, 7-3-1 Hongo, Bunkyo-ku, Tokyo 113-0033, Japan,* [2]*Department of Gastroenterology, Graduate School of Medicine, University of Tokyo, 7-3-1 Hongo, Bunkyo-ku, Tokyo 113-8655, Japan and* [3]*Second Department of Internal Medicine, Wakayama Medical University, Kimiidera 811-1, Wakayama 641-8509, Japan*

It has been repeatedly reported that endothelin-3 (ET-3) is expressed by gastrointestinal mesenchymes, and that paracrine signaling between ET-3 and its receptor plays an essential role in controlling differentiation of the enteric nervous system in the gut, especially in the colon. However it remains to be solved whether ET-3 plays a role in regulating the growth of gastrointestinal epithelial cells. We have previously reported culture systems for forestomach, glandular stomach and duodenal epithelial cells, but a system for colonic epithelial cells has not been established. In the present study, we examined optimal culture conditions for colonic epithelial cells, and examined whether ET-3 affects the growth of gastrointestinal epithelial cells, with special reference to colonic cells. We found that ET-3 dose-dependently and region-specifically stimulated their growth in primary culture: colonic epithelial cells were most responsive, followed by duodenal and glandular stomach epithelial cells. Reverse transcription–polymerase chain reaction analysis showed that ET-3 and a receptor for ET-3 were expressed by both colonic mesenchymes and epithelia, but the levels were much higher in mesenchymes than in epithelia. These results suggest that ET-3 plays an important role in the growth control of colonic epithelial cells, possibly by mediating epithelial–mesenchymal interactions.

Key words: colon, duodenum, endothelin-3, epithelial–mesenchymal interaction, primary culture.

Introduction

Endothelin (ET) was discovered by Yanagisawa *et al.* (1988) on the basis of its vasoconstrictive activity. Two other isoforms including ET-3, which also displayed vasoactive properties, were discovered later. The effects of ET are mediated by at least two distinct receptors, types A (ET_A) and B (ET_B), which bind ET at different affinities. ET_B binds all three ET equally, while ET_A preferentially binds ET-1 (for review, see Levin 1995). Targeted inactivation of *ET-3* has revealed an unexpected role of the ET-3/ET_B interaction in the differentiation of the enteric nervous system (Baynash *et al.* 1994). Also, mice with a disruption of ET_B (Hosoda *et al.* 1994) have a recessive aganglionic megacolon phenotype. The same pathological phenotype is observed in Hirschsprung disease, a neurocristopathy sometimes associated with *ET-3*/ET_B mutations (Gabriel *et al.* 2002).

Organ distribution of *ET* mRNA has been studied. Firth and Ratcliffe (1992) reported that *ET-3* is expressed in a wide variety of organs, including brain, kidney, lung, spleen, stomach, and intestine in adult rats, but it remains to be examined whether it is expressed by epithelial and/or mesenchymal tissues. By using *in situ* hybridization, Leibl *et al.* (1999) showed that *ET-3* was only expressed by intestinal mesenchymes, with the greatest level in the cecum in fetal mice. This suggests that production of ET-3 by the intestinal mesenchyme acts by a paracrine mechanism to stimulate innervation in the intestine by neural crest cells. Such localized expression of *ET-3* was also found and a similar mechanism is suggested in human embryos (Brand *et al.* 1998).

Gastrointestinal epithelium is one of the most actively renewing tissues in the body. Proliferating stem cells are localized in a specialized area in the organ (in

*Author to whom all correspondence should be addressed. Present address: Department of Molecular Oncology, Graduate School of Medicine and Dentistry, Tokyo Medical and Dental University, 1-5-45 Yushima, Bunkyo-ku, Tokyo 113-8519, Japan.
Email: hfukama.monc@tmd.ac.jp

Received 21 July 2005; revised 10 August 2005; accepted 23 August 2005.

the crypt in intestines, and in the gland neck in fundic glands), and most postmitotic epithelial cells migrate upwards to differentiate into specialized cells (absorptive and goblet cells in intestines, and surface mucous cells in the glandular stomach) and to exhibit apoptosis in 4–5 days. These features make the gastrointestinal epithelial cells an excellent model for studying the relationship between cell proliferation, differentiation and morphogenesis. However the control mechanism of their proliferation and differentiation has not been fully understood.

In the fetal rat colon, the epithelium is simple columnar at 13 days of gestation, but it soon becomes stratified by rapid proliferation. At 16–17 days, epithelial cells are undifferentiated and homogeneous, with proliferating cells evenly distributed in the stratified epithelium. Thereafter mitotic cells become localized in the lower layer near the mesenchyme. At about 18–19 days, intraepithelial spaces are connected with the colonic lumen, and the stratified epithelium is transformed into a simple columnar one with primitive crypts (Eastwood & Trier 1974; Brackett & Townsend 1980). Such epithelial morphogenesis can also be found in the glandular stomach and small intestine. Thus 16.5 day fetal gastrointestinal epithelia may be ideal materials in studying the proliferation and differentiation of gastrointestinal epithelial cells.

The importance of epithelial–mesenchymal interactions on the development of gastrointestinal organs has been repeatedly reported. We and others have demonstrated that mesenchymes/stromas affect proliferation and differentiation of intestinal epithelial cells in culture (Fukamachi & Takayama 1980; Kedinger *et al.* 1986; Kedinger *et al.* 1987; Simo *et al.* 1992; Sanderson *et al.* 1996), but the mechanism of interaction has not been fully understood, although several factors including hepatocyte growth factor (Fukamachi *et al.* 1994b) and laminin extracellular matrix (Plateroti *et al.* 1997) have been shown to mediate it. Since *ET-3* is strongly expressed in gut mesenchymes in fetal mice, it is probable that ET-3 affects the growth and differentiation of gastrointestinal epithelial cells, by mediating epithelial–mesenchymal interaction.

To assess the validity of this hypothesis, it is essential to examine the effect of ET-3 on the growth of gastrointestinal epithelial cells in primary culture, but the culture system for colonic epithelial cells has not been fully established, though we have previously reported systems for duodenal (Fukamachi 1992), glandular stomach (Tsukada *et al.* 1998) and forestomach (Fukamachi *et al.* 1995) epithelial cells.

In the current report, we describe a primary culture method for colonic epithelial cells, where the cell number increased more than 7-fold in 4 days. Using this system, we found that ET-3 strongly stimulates the growth of colonic epithelial cells, but the growth of duodenal and glandular stomach epithelial cells was only weakly stimulated by ET-3. We also found that both *ET-3* and the receptor for ET-3 are expressed by gastrointestinal tissues but that the levels are greater in mesenchymes than in the epithelia in the colon and duodenum. We thus speculate that ET-3 secreted from colonic mesenchymes controls overlying epithelial growth by mediating epithelial–mesenchymal interaction.

Materials and methods

Primary culture of colonic epithelial cells

Colonic epithelial tissues were obtained from 16.5 day fetuses of F344/Du rats (Charles River Japan, Tokyo, Japan), and cultured with a method essentially similar to that used for duodenal epithelial cells (Fukamachi 1992). Briefly, epithelial tissues were separated from mesenchymes by the aid of forceps under a dissecting microscope after collagenase treatment. They were further treated with collagenase and hyaluronidase, and smaller tissue fragments were obtained by repeated pipetting with a Pasteur pipette. After thorough washing with Hanks' solution to remove enzymes, they were seeded on rat tail collagen gel (Imagawa *et al.* 1984) in Ham's F-12 medium (Sigma, St Louis, MO, USA) supplemented with bovine serum albumin (1 mg/mL; Sigma), epidermal growth factor (EGF; Upstate Biotechnology, Lake Placid, NY, USA), insulin (Sigma), cholera toxin (List Biol. Lab., Campbell, CA, USA), transferrin (Sigma), hydrocortisone (Sigma), bovine pituitary extract (BPE; Kyokuto Pharmaceutical, Tokyo, Japan), and horse serum (Handai Biken, Osaka, Japan), and incubated in a humidified atmosphere of 5% CO_2 in air at 37°C. The cell number was determined by MTT assay as has been reported (Fukamachi 1992). To allow comparison of separate experiments, cell numbers were expressed as a percentage by regarding the cell number in the standard culture condition as 100%.

Effect of ET-3 on the growth of gastrointestinal epithelial cells

The effect of ET-3 on the growth of forestomach, glandular stomach, duodenal and colonic epithelial cells was compared in primary culture. Forestomach and glandular stomach epithelial cells were cultured in a medium used for glandular stomach epithelial cells (Tsukada *et al.* 1998), and duodenal and colonic epithelial cells were grown in a medium for duodenal

epithelial cells (Fukamachi 1992), to compare the growth of the epithelial cells from neighboring organs in the same culture condition. The cell number was determined by MTT assay, and the data were analyzed using Student's *t*-test, and differences were considered significant when $P < 0.05$.

RNA extraction and reverse transcription–polymerase chain reaction

The epithelial and mesenchymal tissues of forestomach, glandular stomach, duodenum and colon were obtained from 16.5 day rat fetuses, and total RNA was extracted from the tissues by Trizol (Invitrogen, San Diego, CA, USA), according the manufacturer's instructions. Approximately 1 μg of total RNA from each tissue was reverse transcribed to cDNA using SuperScript II Reverse Transcriptase (Invitrogen) and the resulting cDNA was subjected to 30 cycles of polymerase chain reaction (PCR) using ExTaq DNA polymerase (Takara, Kyoto, Japan). The following oligonucleotide primer pairs were used for the PCR reactions (expected product size in parentheses): ET-3 (477 bp), 5′-TTCTCGGGCTCACAGTGACC-3′ (sense) and 5′-GCTGGTGGACTTTATCTGTCC-3′ (antisense); ET_A (418 bp; Shigematsu *et al.* 1998), 5′-CAGATCCACATTAAGATGGG-3′ (sense) and 5′-GGAGATCAATGACCACGTAG-3′ (antisense); and ET_B (475 bp; Wang *et al.* 1996) 5′-TTCACCTCAGCAGGATTCTG-3′ (sense) and 5′-AGGTGTGGAAAGTTAGAACG-3′ (antisense). G3PDH was used as a control to compare tissues of different sizes and to compensate for varying efficiencies of extraction and reverse transcription (RT) as described previously (Matsubara *et al.* 1998). The PCR products thus generated were separated by electrophoresis on 2.0% agarose gels in 0.5x TAE buffer.

Results

Growth of colonic epithelial cells in primary serum-free culture

When fetal rat colonic tissues were treated with collagenase, epithelial and mesenchymal components could be separated with the aid of forceps. As shown in Fig. 1A, pure epithelial tissues with few contaminating mesenchymal cells could be obtained, and were used for primary culture. It was essential to seed small tissue fragments for culture, since neither single epithelial cell nor large tissue fragments would attach to the substratum. When small epithelial fragments were seeded on collagen gels, most (> 90%) of them attached to the substratum, and proliferated

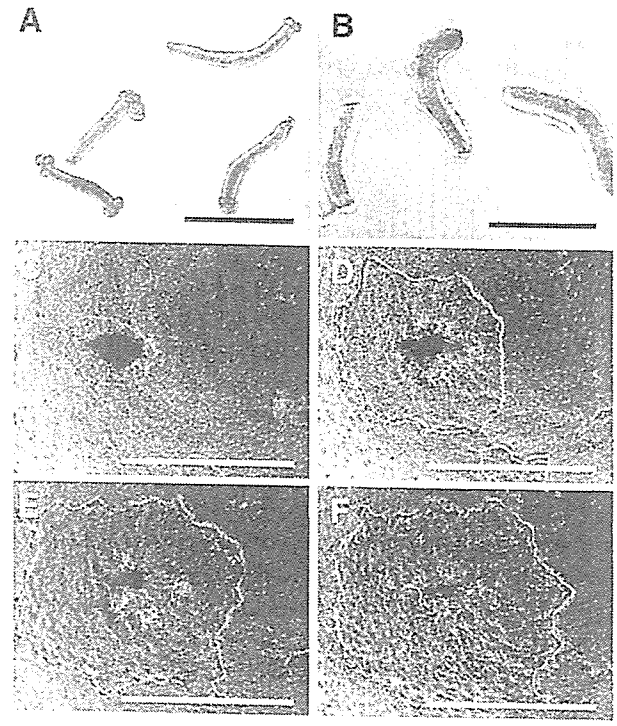

Fig. 1. Phase contrast micrographs of fetal rat colonic tissues. (A) Epithelial and (B) mesenchymal tissues just after separation by collagenase treatment. Note that no contaminating cells could be found in both tissues. (C–F) Growth of colonic epithelial cells in primary culture on days (C) 1, (D) 2, (E) 3 and (F) 4, showing sequential changes of the same tissue fragment in culture. Note that the cells grew rapidly from days 1–3, but cell growth slowed down from days 3–4. Bars, 1 mm.

rapidly in the first 4 days under optimal culture conditions (see below). These epithelial cells attached closely to each other, and exhibited typical epithelial morphology with distinct margination of cell sheets (Fig. 1C–F). The epithelial nature of the cells was confirmed by the presence of cytokeratin (data not shown). Collagen gel was necessary for the attachment and proliferation of colonic epithelial cells: without collagen gels, less than 5% of the cells attached to and proliferated on plastic substratum, whereas approximately 50% of the cells attached to and proliferated on a dried collagen substratum. This is similar to the properties of duodenal epithelial cells (Ichinose *et al.* 1997). We have previously reported that collagen gel is superior to basement membrane components including laminin and type IV collagen in inducing growth of gastrointestinal epithelial cells (Ichinose *et al.* 1997). Thus in the present experiment, collagen gel was used as a substratum. The epithelial cells ceased to proliferate on days 4–5 in culture, and some cells began to degenerate on day

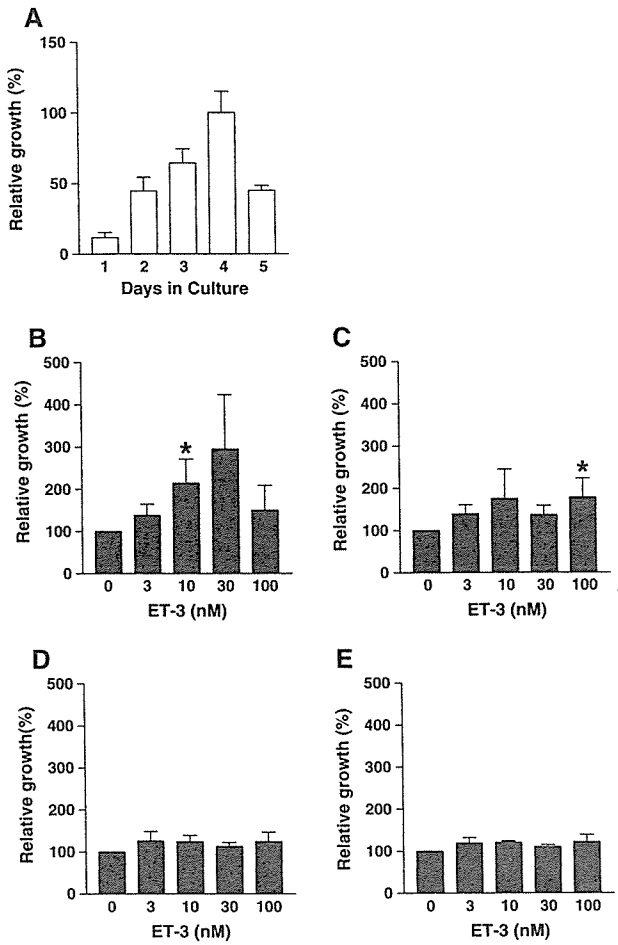

Fig. 2. (A) Growth of colonic epithelial cells in primary culture under optimal conditions. Each point represents mean ± SE of six independent experiments. (B–E) Effect of ET-3 on the growth of (B) colonic, (C) duodenal, (D) glandular stomach and (E) forestomach epithelial cells in primary culture. The cell number was determined on day 4 in culture, and data are summarized from three to six independent experiments. Asterisks indicate that values are significantly greater than controls.

5 (Fig. 2A). Attempts have been made to subculture colonic epithelial cells, but so far they have not been successful. Considering that postmitotic cells exhibit apoptosis within 4–5 days after they leave the stem cell zone *in vivo*, we speculate that it is a physiological reaction that the colonic epithelial cells ceased to proliferate on days 4–5 in culture.

The proliferation of colonic epithelial cells in culture was quantitatively measured by an MTT assay. We have previously shown that there is a good correlation between the cell number in a well and the amount of formazan produced by the cells in the range of 1×10^3 to 5×10^4 cells (Fukamachi 1992). The effect of growth factors on the proliferation of colonic epithelial cells was quantitatively examined, and optimal culture condition was determined. The cells proliferated most extensively when cultured in F-12 supplemented with EGF (10 ng/mL), insulin (30 μg/mL), cholera toxin (200 ng/mL), transferrin (10 μg/mL), hydrocortisone (2 μg/mL) and BPE (100 μg/mL; Table 1). These factors synergistically induced epithelial proliferation. This is clearly shown by Table 2, where the lack of any one of six factors severely inhibited the epithelial proliferation. Serums were not used since any lot of serum examined (a total of 10 lots, including fetal bovine serum, bovine serum and horse serum) inhibited the colonic epithelial growth (the cell number was decreased to 43 ± 18% of the controls by adding 10% serum into the complete medium).

ET-3 dose-dependently and region-specifically stimulated the growth of gastrointestinal epithelial cells

The effect of ET-3 on the growth of colonic, duodenal, glandular stomach and forestomach epithelial cells was examined in primary culture. To examine whether forestomach and glandular stomach epithelial cells respond differently to ET-3, they were cultured in the same medium optimum for glandular stomach epithelial cells. In case of duodenal and colonic epithelial cells, their response to ET-3 was compared in a medium for duodenal epithelial cells, since BPE suppressed the growth of duodenal epithelial cells (Fukamachi *et al.* 1995).

The cell number was determined on day 4 when it was greatest in the culture of colonic epithelial cells, and rapid cell growth was ceased in the cultures of duodenal (Fukamachi 1992) and glandular stomach (Fukamachi *et al.* 1994a) epithelial cells. ET-3 dose-dependently stimulated the growth of colonic and duodenal epithelial cells, and their numbers were increased about 3-fold and 1.8-fold by adding 30 nM and 100 nM ET-3, respectively (Fig. 2B,C). In contrast, ET-3 only weakly stimulated the growth of glandular stomach and forestomach epithelial cells (Fig. 2D,E). These results indicate that colonic epithelial cells are the most responsive to the growth-stimulating effect of ET-3, followed by duodenal and glandular stomach epithelial cells. We thus conclude that ET-3 may play an important role in controlling gastrointestinal epithelial growth in development, especially in the colon.

ET-3 *and its receptor were expressed by both mesenchymal and epithelial tissues in the developing gut*

Next, we examined whether *ET-3* and receptors for ET-3, were expressed in the fetal rat gastrointestinal

Table 1. Combinations and concentrations of growth factors which induce maximal growth of gastrointestinal epithelial cells in primary culture

Growth factors	Forestomach	Glandular stomach	Duodenum	Colon
Horse serum (%)	10	10	–	–
BPE (μg/mL)	100	100	–	100
EGF (ng/mL)	10	10	20	10
Cholera toxin (ng/mL)	300	300	200	200
Hydrocortisone (μg/mL)	1	3	3	2
Insulin (μg/mL)	–	3	30	30
Transferrin (μg/mL)	–	–	100	10

The best concentration of a factor was determined by changing its concentration while the concentration of other factors was kept constant. Data for forestomach, glandular stomach and duodenum are from Fukamachi *et al.* (1995).

–, No effect or inhibitory for epithelial growth. BPE, bovine pituitary extract; EGF, epidermal growth factor.

Table 2. Effect of depletion of a growth factor from the complete media on the growth of gastrointestinal epithelial cells in primary culture (cell numbers are expressed as percentage by regarding the cell number in complete media as 100%)

Growth factors	Forestomach	Glandular stomach	Duodenum	Colon
Horse serum	16 ± 10(5)†	57 ± 25(5)	–	–
BPE	54 ± 11(5)	48 ± 9(5)	–	59 ± 22(5)
EGF	75 ± 7(5)	79 ± 15(5)	34 ± 17(8)	72 ± 10(6)
Cholera toxin	61 ± 11(5)	56 ± 6(59)	28 ± 27(7)	55 ± 23(5)
Hydrocortisone	48 ± 10(7)	60 ± 16(5)	24 ± 19(9)	69 ± 28(8)
Insulin	–	85 ± 9(5)	59 ± 49(8)	58 ± 14(6)
Transferrin	–	–	37 ± 19(7)	59 ± 16(6)

†Mean ± SD (number of experiments). Data for forestomach, glandular stomach and duodenum are from Fukamachi *et al.* (1995).

–, No effect or inhibitory for epithelial growth. BPE, bovine pituitary extract; EGF, epidermal growth factor.

tract by RT–PCR. It was difficult to measure the concentration of ET-3 protein in the developing gastrointestinal tissues because the tissues were too small to obtain reproducible results, but reproducible results could be obtained at the level of mRNA. As shown in Fig. 3, *ET-3* and ET_B, a receptor for ET-3, were expressed by both mesenchymes and epithelia of gastrointestinal organs. In the colon and duodenum, their levels were greater in mesenchymes than in epithelia, while their levels were similar in glandular stomach and forestomach. In contrast, ET_A, a receptor for ET-1, was expressed exclusively by gastrointestinal mesenchymes, and only a slight expression could be found in the overlying epithelial cells. Considering that ET-3 significantly stimulated colonic epithelial growth, we suppose that ET-3 secreted from the colonic mesenchyme regulates the growth of overlying epithelial cells, by mediating epithelial–mesenchymal interaction.

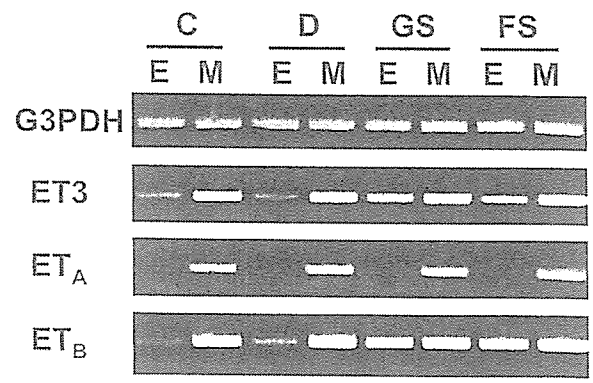

Fig. 3. Expression of *ET-3*, ET_A and ET_B genes in epithelial (E) and mesenchymal (M) tissues of colonic (C), duodenal (D), glandular stomach (GS) and forestomach (FS) tissues from 16.5-day fetal rats. Expression of mRNA for *ET-3*, ET_A, and ET_B was assessed by RT–PCR and normalized according to the expression of G3PDH.

Discussion

In the present study, we found that colonic epithelial cells from fetal rats proliferated in primary culture in a chemically defined serum-free medium in the absence of mesenchymal cells. Using this system, we quantitatively examined the effect of growth factors on the proliferation of colonic epithelial cells *in vitro*, and found that EGF, insulin, cholera toxin,

transferrin, hydrocortisone and BPE synergistically stimulated their growth while serum inhibited it. We have previously reported that EGF, insulin, cholera toxin, transferrin and hydrocortisone stimulate, and serum severely inhibits, growth of duodenal epithelial cells in primary culture (Fukamachi 1992). Thus, colonic and duodenal epithelial cells are very similar in their responsiveness to growth factors; however, there are some differences. BPE inhibits the growth of duodenal epithelial cells but stimulates that of colonic cells. Also, duodenal epithelial cells are more sensitive than colonic ones to the growth-inhibitory effects of serum. In previous studies, colonic epithelial cells were almost always grown in the presence of serum, and it has been difficult to quantify the effects of growth factors on their proliferation (Moyer & Aust 1984; Buset *et al.* 1987; Chopra *et al.* 1987; Whitehead *et al.* 1987; Kaeffer *et al.* 1997; Sugiyama *et al.* 1998). This may be due to the growth-inhibitory effect of serum. Because our culture system does not employ serum, it should be useful for future studies on the mechanisms by which colonic epithelial growth is controlled.

Using the system, we found that ET-3 significantly stimulated gastrointestinal epithelial growth. The growth-promoting activity of ET-3 has been reported on various cell types, including vascular smooth muscle cells, fibroblasts, astrocytic glial cells, osteoblastic cells, melanocytes, and mesangial cells (Battistini *et al.* 1993), but the effect of ET-3 on intestinal epithelial growth has not been examined. Using IEC-6 and IEC-18 small intestinal epithelial cell lines, Shigematsu *et al.* (1998) reported that these cells expressed *ET-1*, ET_A and ET_B, but not *ET-3*, and that exogenously added ET-1 induced a slight proliferative response in both cells. They did not examine the effect of ET-3 on the cells. Thus, our current report may be the first demonstration that ET-3 has mitogenic activity on intestinal epithelial cells.

In the present study, we found that ET-3 region-specifically stimulates the growth of gastrointestinal epithelial cells, with the greatest response from the colonic epithelial cells, followed by duodenal and glandular stomach epithelial cells. We thus speculate that there is a head-to-tail gradient in the gastrointestinal epithelial cells which controls epithelial response to ET-3, with the greatest response in the caudal region (colon) and the least response in the rostral region (glandular stomach). We have previously reported similar head-to-tail gradients which control the epithelial response to growth factors and substrata in the developing gastrointestinal epithelial cells (Fukamachi *et al.* 1995). The present result is consistent with the previous one. The nature of this gradient remains to be determined. Roberts *et al.* (1995) reported that sonic hedgehog from the endoderm plays a role in inducing a nested pattern of *Hox* gene expression in the mesoderm surrounding the hindgut, and that regionalized medoderm then instructs the endodermal tube to become the different organs of the digestive tract. Recently, canonical Wnt signaling and its inhibition have been shown to be essential for the development of gastric epithelial cells (Kim *et al.* 2005). It remains to be examined how ET-3 is involved in the specification and differentiation of gastrointestinal organs in the developing intestine.

In the present study, we found that *ET-3* and ET_B were expressed by both gastrointestinal epithelia and mesenchymes while ET_A, the receptor for ET-1, was exclusively expressed by mesenchymal tissues. That *ET-3* is expressed by intestinal mesenchymes has been repeatedly demonstrated in human and mouse fetuses (Brand *et al.* 1998; Leibl *et al.* 1999). Our finding that *ET-3* is expressed by colonic and duodenal mesenchymes is consistent with these previous studies, and together they suggest that ET-3 is an important mesenchyme-derived growth factor that controls intestinal epithelial growth in developing mammalian fetuses.

In the glandular stomach and forestomach whose epithelial growth was only scarcely stimulated by ET-3, both *ET-3* and ET_B, were expressed at a high level. Thus the level of ET_B expressed in the epithelial cells did not correlate with their responsiveness to the growth-stimulating effect of ET-3. It is possible that the growth-promoting activity of ET-3 in culture was suppressed by serum and/or BPE supplemented in the culture medium for glandular stomach and forestomach epithelial cells. It is more probable that ET-3 may play other roles such as control of epithelial differentiation in these organs. It is interesting to note that ET-1/ET_A signal transduction has recently been shown to be involved in branchial arch development (Fukuhara *et al.* 2004). It is a problem for the future how ET-3 is concerned in the differentiation and morphogenesis of the gastrointestinal organs.

It is well established that a targeted disruption of *ET-3* or ET_B results in aganglionic megacolon and pigmentary disorders in mice (Baynash *et al.* 1994; Hosoda *et al.* 1994). However, the proliferation and differentiation of colonic epithelial cells in these transgenic mice have not been fully examined mostly because they usually die several weeks after birth, before maturation. It is likely that colonic epithelial growth is altered in the transgenic mice given our finding that ET-3 affects the growth of colonic epithelial cells *in vitro*. Further studies are needed to confirm whether the colonic epithelial growth is altered in these transgenic mice in development.